Progress In Electromagnetics Research, Vol. 128, 229–248, 2012

IMPROVED THERMAL ABLATION EFFICACY USING MAGNETIC NANOPARTICLES: A STUDY IN TUMOR PHANTOMS

S. García-Jimeno[1], R. Ortega-Palacios[2], M. F. J. Cepeda-Rubio[2], A. Vera[2], L. Leija[2], and J. Estelrich[1, 3, *]

[1]Departament de Fisicoquímica, Facultat de Farmàcia, Universitat de Barcelona, Avda. Joan XXIII, 08028 Barcelona, Catalonia, (Spain)

[2]Electrical Engineering Department, Bioelectronics Section, CINVESTAV-IPN, Mexico D.F., Mexico

[3]Institut de Nanociència i Nanotecnologia, IN^{2}UB, Universitat de Barcelona, (Spain)

Abstract—Magnetic heating used for inducing hyperthermia and thermal ablation is particularly promising in the treatment of cancer provided that the therapeutic temperature is kept constant during the treatment time throughout the targeted tissue and the healthy surrounding tissues are maintained at a safe temperature. The present study shows the temperature increment produced by different concentrations of magnetic nanoparticles (ferrofluid and magnetoliposomes) inside a phantom, after irradiating tissue-mimicking materials (phantoms)with a minimally invasive coaxial antenna working at a frequency of 2.45 GHz. This frequency was chosen because maximum dielectric loss of water molecules begins at 2.4 GHz and because this is an ISM (industrial, scientific and medical) frequency. Temperature sensors were placed inside and outside the tumor phantom to assess the focusing effect of heat produced by nanoparticles. Results have shown that the temperature increments depend on the nanoparticles concentration. In this way, a temperature increment of more than 56°C was obtained with a ferrofluid concentration of 13.2 mg/mL, whereas the increment in the reference phantom was only of $\approx$ 21°C. Concerning the magnetoliposomes, the temperature achieved was similar to that obtained with the ferrofluid but at a lesser concentration of nanoparticles. These results

Received 1 February 2012, Accepted 27 March 2012, Scheduled 30 May 2012

* Corresponding author: Joan Estelrich (joanestelrich@ub.edu).

demonstrate that it is possible to achieve higher temperatures and to focus energy where the nanoparticles are located.

1. INTRODUCTION

Magnetic nanoparticles (MNPs) for medical applications have been developed in recent years. Since MNPs have magnetic features that are not present in most biological materials, they can be applied in special medical techniques such as cell separation, separation of biological materials using magnetically labeled beads, immunoassays, magnetic resonance imaging (MRI), drug delivery, thermal marking to improve the tumor detection capacity of thermography, and hyperthermia therapy [1–7].

Hyperthermia is a cancer treatment used to enhance the effects of already established therapies, such as radiotherapy and chemotherapy. The most important requirement for the use of hyperthermia in cancer therapy is to locally increase and maintain temperature within cancer cells above 41°C while surrounding healthy tissues remain at safe temperatures. Under this general concept of hyperthermia, one can distinguish between hyperthermia (when temperature is between 40°C and 44°C) [8, 9] and thermal ablation if temperature exceeds 50°C [10]. When thermal energy increases the tissue temperature above 40°C, normal cellular processes become deactivated in a dose-dependent manner, which eventually may result in the death of cells. In thermal ablation, in contrast, cells or tissues show areas of extensive necrosis [11].

Electromagnetic radiation can be used to induce hyperthermia. The electromagnetic energy must be directed from an external source and it must penetrate normal tissue. Minimally invasive antennas can be also used in electromagnetic hyperthermia; in this case, the antenna is inserted in the tissue and is in direct contact with the tissue. Although the efficacy of electromagnetic hyperthermia has been proven in numerous clinical trials, it has not gained wide acceptance. The major technical problem with electromagnetic hyperthermia is the difficulty of heating the target tumor at the desired temperature without damaging the surrounding tissues. MNPs of various types may address this issue through intracellular hyperthermia or ablation; i.e., by driving submicron magnetic particles inside the tumor and then making them generate heat under an alternating magnetic field [12].

In order to generate heat, as described above, nanoparticles with superparamagnetic properties are inserted into the tumor and then they are exposed to an electromagnetic field (EMF) which operates at radio frequencies (RF) or in the microwave (MW) range. In this

way magnetic and electrical energy is transformed into heat. Polar molecules interact with electric fields and cause frictional heating while magnetic loss is attributed to Néel relaxation due to rapidly alternating magnetic dipole moments. Brownian relaxation, which occurs due to nanoparticle rotation, results in friction between particles and surrounding fluids. In MNPs, Brownian and Néel relaxation depends on particle size (an average value of $\sim 15\,\text{nm}$)and composition [13, 14].

Different equations describe the interaction of electromagnetic fields with tissue; this interaction causes heating in biological tissues under certain conditions (applied power, exposure time). The bioheat transfer equation (BHTE) is used to describe the temperature evolution in biological tissues. The BHTE can be written as:

$$\rho_t C_t \frac{\partial T}{\partial t} = \text{div}\left(k\nabla T\right) + \omega_b \rho_b C_b \left(T_b - T\right) + Q_{met} + Q_{ext}, \tag{1}$$

where ρ_t, C_t, and k, are the density, specific heat and thermal conductivity of the tissue, respectively; ρ_b, C_b, and ω_b are the density, specific heat and perfusion rate of blood, respectively; T_b is the arterial blood temperature; Q_{met} is the heat source from metabolism, and Q_{ext} is the absorbed power density which can be written as:

$$Q_{ext} = \frac{1}{2}\sigma_t \left|E\right|^2, \tag{2}$$

where σ_t is the electrical conductivity of the tissue and E is the electric field generated by the electromagnetic source, in our case the antenna. By analyzing Eq. (2), it is evident that only the E field is taken into account to achieve the temperature increment in tissues and tumors. Although the antenna generates E and H fields, the last one is neglected because tissues are considered as nonmagnetic. However, when magnetic nanoparticles are injected into tumors, nanoparticle magnetic properties are intensified, and consequently, the H field also is involved in the heating process.

On the other hand, if magnetic nanoparticles are concentrated inside tumors, the absorbed power density is given by [15]:

$$Q_{ext} = \pi\mu_0\chi'' f H^2, \tag{3}$$

where μ_0 is the permeability of free space, χ'' is the imaginary part of the magnetic susceptibility, f is the frequency of the alternating magnetic field, and H is the magnetic field amplitude. From Eq. (3), it can be seen that temperature increments are proportional to the square of the amplitude of the H field intensity. In this case, the E and H fields can be used as sources for heating. Substituting Eqs. (2) and (3) in Eq. (1), the BHTE can be rewritten as:

$$\rho_t C_t \frac{\partial T}{\partial t} = \text{div}\left(k\nabla T\right) + \omega_b \rho_b C_b \left(T_b - T\right) + Q_{met} + \frac{1}{2}\sigma_t |E|^2 + \pi\mu_0\chi'' f H^2 \tag{4}$$

From Eq. (4), it can be observed that the heating effect is produced by both the electric and magnetic fields generated by the applicator; i.e., the heating effect produced by the antenna depends not only on the square of E field but also on the square of H field. For this reason, the heating efficiency of the approach being reported here is expected to be higher compared with that obtained without using nanoparticles, where just the magnetic field is taken into account for heating [16]. The distribution of temperature increment in phantoms with different concentrations of magnetic particles has been analyzed in this study in order to test the hyperthermic effect of magnetic nanoparticles, and to observe the behavior of temperature increment in the deep regions of the tumor tissue as well as the dependence of the concentration of magnetic particles in it.

Currently, MNPs consisting of iron oxide nanoparticles are widely used. Among the materials potentially suitable for use in thermal therapy, magnetite has been considered the best from the standpoint of magnetic properties and biocompatibility [17]. To a large extent, the morphological, structural, and magnetic profiles of nanoparticles determine their suitability as magnetic hyperthermia/ablation agents. Such information is therefore of paramount importance when attempting to produce the temperatures required with a minimal magnetic particle concentration and also to avoid damaging surrounding normal tissue through overheating.

As mentioned above, one important issue for hyperthermia treatment is to know how the temperature increases in tumor tissue, as well as whether the heat is focused inside the tumor. One challenge of assessing induced energy generation in animal tissue is the technical difficulty of visualizing MNPs. To date, gel phantoms have been the only transparent porous materials that are equivalent to animal tissue for *in vitro* studies, despite the fact that gels are homogeneous in comparison to the complicated morphology of a tumor.

In this study, increments of temperature and heat focusing were determined by using a phantom as a tumor model and MNPs based on ferrofluid and magnetoliposomes (MLs) at different concentrations. The phantom was made of a mixture of different components in order to represent the thermal and electromagnetic properties of human tissues [14, 18]. The ferrofluid was based on magnetite stabilized by polyethylene glycol (PEG), and the MLs were liposomes encapsulating the ferrofluid. A minimally invasive coaxial antenna was used to irradiate the phantom.

2. MATERIALS AND METHODS

2.1. Materials

Soybean phosphatidylcholine (PC), a zwitterionic phospholipid (Lipoid S-100), was a gift from Lipoid (Ludwigshafen, EU). Ferric chloride hexahydrate ($Cl_3Fe.6H_2O$), ferrous chloride tetrahydrate ($Cl_2Fe.4H_2O$) and cholesterol (CHOL)were purchased from Sigma-Aldrich (St. Louis, MO, USA). PEG of 6000 Da molecular weight was from VWR International (Barcelona, EU). Agarose (Ultrapure^{TM} agarose) was purchased from Invitrogen (Mexico, D.F.). All other reagents were of analytical grade and were from Panreac (Barcelona, EU). Deionized Millipore Milli-Q water was used in all the experiments. A strong neodymium-iron-boron ($Nd_2Fe_{12}B$) magnet (1.2 T) was obtained from Halde GAC (Barcelona, EU).

2.2. Preparation and Characterization of Magnetic Nanoparticles

Ferrofluid was prepared using the co-precipitation method in the presence of excess PEG. Briefly, once the polymer was dissolved in water, a 1:2 molar ratio mixture of $FeCl_2/FeCl_3$ was added. When the PEG and iron salts were well dissolved, an ammonia solution was added drop-wise while being stirred. After this, the ferrofluid was poured into a beaker and the vessel was placed on a permanent magnet. The ferrofluid was washed with water by decanting the supernatant in order to eliminate excess PEG. Finally, PEG coated particles were dispersed in water and the resulting suspension was sonicated for 10 min at room temperature and 100% of the ultrasonic power (Transsonic Digital Bath sonifier, Elma, EU).

MLs were obtained by extrusion [19]. A mixture of PC/CHOL (4:1 molar ratio) dissolved in chloroform/methanol (2:1, v/v) was evaporated until a film was formed. This film was hydrated with the appropriate amount of a mixture of water and ferrofluid (FF) to give a lipid concentration of 16 mmol/L. Multilamellar liposomes were formed by gentle sonication and vortexing. After this, multilamellar liposomes were extruded at room temperature in a Liposofast device (Avestin, Canada) through two polycarbonate membrane filters of 0.2-µm pore size, a minimum of 9 times. Finally, unilamellar MLs were obtained.

The morphology of the samples was studied by transmission electron microscopy (TEM) using a Jeol 1010 microscope at an accelerating voltage of 80 kV. Images were recorded with a Megaview III camera, and acquisition was accomplished with Soft-Imaging software (SIS, Münster, EU). The hydrodynamic diameter of the MNPs

was determined by dynamic light scattering (DLS) at 90° with a Zetasizer Nano (Malvern, EU) at 25°C. Particle size distribution was designated using the polydispersity index (PI), which ranged from 0.0 for an entirely monodisperse sample to 1.0 for a polydisperse sample. Iron content of the ferrofluid and MLs was determined by inductively-coupled plasma-optical emission spectrometry (ICP-OES) using Perkin Elmer equipment (Optima 3200RL). Magnetic measurements were made on a superconducting quantum interference device (SQUID) magnetometer (Quantum design MPMS XL) at room temperature. The external magnetic field was swept from +5000 to −5000 Oe, and then back to +5000 Oe.

2.3. Preparation and Characterization of Agarose Tumor Phantoms

A phantom was prepared by dispersing agarose, tridistilled water, ethanol and NaCl (0.1 M) to obtain a permittivity near to the values of breast carcinoma at 2.45 GHz. At this frequency, tumor permittivity is around 60 and its conductivity is about 2.5 S/m; the phantom mimicking the tumor had a permittivity of 55.88 and a conductivity of 2.88 S/m. The mixture was then heated to 80°C, until the agarose was completely dissolved. The solution was then poured into a transparent container and cooled to room temperature (25°C) until solidification occurred.

In order to maintain the MNPs in a specific place inside the phantom, they were concentrated in small spheres of agarose. Each sphere was made of tridistilled water, 0.006 g/mL of agarose and several concentrations of magnetite. Two sizes of spheres were used: some with a volume of 2.5 mL and 1.68 cm in diameter, and others with a volume of 5 mL and 2.12 cm in diameter. For the spheres of 2.5 mL, the following concentrations of magnetite were used: 0.0 (reference phantom), 2.2, 4.4, 5.5, 8.8 and 13.2 mg/mL (for the ferrofluid) and 1.2 mg/mL when the sphere was made with MLs. For spheres of 5 mL, only one concentration of magnetite in ferrofluid (8.8 mg/mL) and MLs (1.2 mg/mL) was used. The spheres were introduced inside the phantom before it was totally solidified.

Electrical properties of the phantom were measured in order to compare them with those of human tissues. Figure 1 shows the experimental setup used to characterize the phantoms that was subjected to a radiation process with the microcoaxial antenna. The phantom permittivity was measured using a dielectric probe kit (85070C, Hewlett Packard, USA). The dielectric probe kit software provided real (ε) and imaginary (ε'') permittivity. Phantom electrical conductivity was obtained from the equation: $\sigma = \varepsilon'' \varepsilon_0 \omega$, where $\omega =$

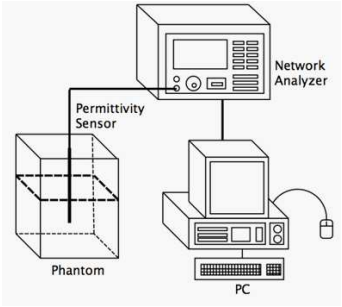

Figure 1. Experimental setup used to measure the electrical properties of the phantom.

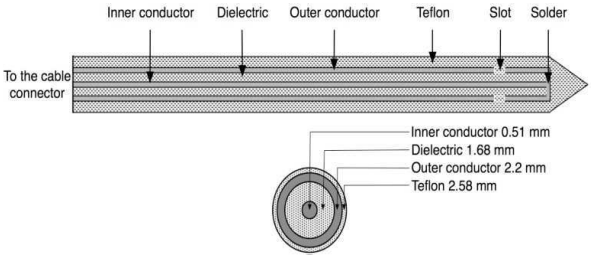

Figure 2. Structure and dimensions of the coaxial antenna.

$2\pi f$ is the angular frequency and f is the frequency of the radiation. It is important to remark that the dielectric probe measurements assume that the sample under test has a permeability of 1 (non-magnetic);this is not true for samples with MNPs, and, in consequence, such values are valid in a qualitative sense. It is important to know the values of the electrical properties because those values are related to the temperature increase (it is possible to enhance heat generation by changing the dielectric properties of tissues).

2.4. Antenna Design

The antenna worked at 2.45 GHz and was based on a 50-Ω UT-085 semi rigid coaxial cable. The entire outer conductor was made of copper and a small ring-shaped slot was carved in it, close to the short-circuited distal tip of the antenna, to allow electromagnetic wave propagation into the tissue. Our antenna had a 1-mm-wide slot, in order to get minimal power reflection. The inner conductor was made of silver-plated copper wire (SPCW) and the coaxial dielectric used was low-loss polytetrafluoroethylene (PTFE). The length of the antenna tip affected power reflection and the shape of the SAR (specific absorption rate)

pattern, and it was adjusted to provide a good trade-off between power reflection and SAR pattern. In addition, the antenna was encased in a PTFE catheter to prevent adhesion of ablated tissue [20]. Figure 2 shows the structure of the antenna, and its inner diameters. It is important to mention that when this kind of antenna is used in clinical trials, it is introduced inside tissues so it is considered as a minimally invasive applicator.

2.5. Microwave Ablation System

The experimental setup consisted of a radiation system and a thermometry system (Figure 3). The radiation system employed a power amplifier SSPA 1.0-2.5-50 W (Aethercomm, Carlsbad, CA, USA) and a microwave generator SML03 2.45-GHz (Rohde & Schwarz, Germany). The thermometry system used fiber-optic thermal probes (Luxtron, Santa Clara, CA, USA) to measure the real-time

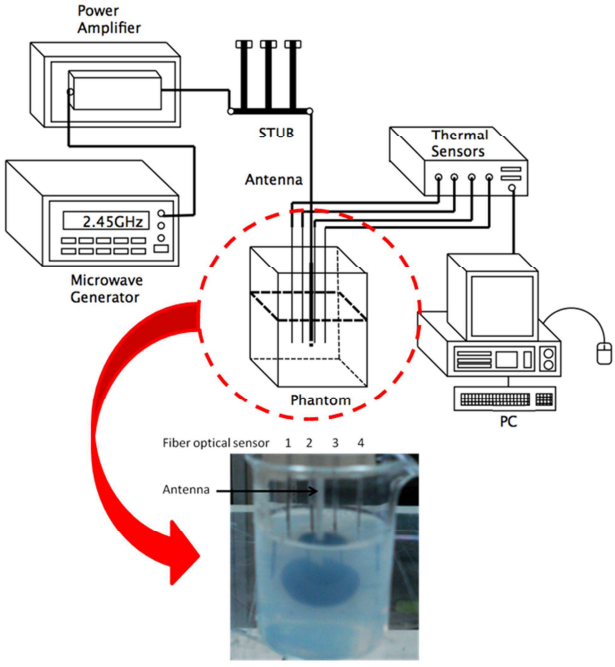

Figure 3. Schematic representation of the radiation and thermometry system. An image of an actual tumor phantom, with FF inside, is shown. Fiber-optic sensors and antenna are embedded in the tumor phantom.

temperature during the microwave ablation (MWA) experiments. The fiber-optic thermal sensors were connected to the M3300 Fluoroptic thermometer (Luxtron) and had a communication link to a computer via an RS-232 serial cable. This experimental setup, used to measure temperature increments inside the muscle phantom and the tumor, has been used in previously described hyperthermia studies [21].

The temperature sensors were placed alongside the antenna, at 0.0 cm, 0.5 cm, 1.0 cm and 1.5 cm, for every experiment. We used a stub between the power amplifier and the antenna to get the best standing wave ratio (SWR), which was measured by a network analyzer (Agilent Technologies, Santa Clara, CA, USA). SWR measurements were carried out with the antenna embedded in the phantom.

The radiation power during the experiments was 10 W and was applied for 5 min. Transmission and reflection power levels were monitored by a power meter PM2002 (Amplifier Research, Souderton, PA, USA). The stub was adjusted so that the reflected power was minimal (SWR near 1.0) and incident power was maximal (10 W). The frequency was fixed at 2.45 GHz. Data was stored every second by using a computer connected to the fluoroptic thermometer.

2.6. Temperature Measurements in Agarose Tumor Phantoms

When the tumor phantom was solid, the glass capillaries and the coaxial antenna were inserted inside the phantom. Once they were placed at the desired position, temperature probes were placed inside the phantom through the glass capillaries. Four temperature sensors were inserted in a horizontal line, with a distance of $\sim$ 0.5 cm between them. The coaxial antenna was inserted at the center of the sphere. A temperature sensor was placed next to the antenna; another sensor was positioned at 0.5 cm from the antenna and the other two sensors were situated at 1.0 cm and 1.5 cm respectively. For the small sphere, diameter of 1.68 cm, the last two sensors were placed outside the MNPs sphere, only in contact with the tumor phantom. For the big sphere, diameter of 2.12 cm, only the outermost sensor was placed outside the MNPs sphere. The antenna was then connected to the stub until coupling between the antenna and power amplifier was achieved; we considered that coupling was attained when measured SWR was near 1.0. Once the coupling was adjusted, microwave radiation was applied for 5 min. The initial temperature of the phantom was controlled at $\sim$25°C, and temperature increments were recorded. Measured temperature was compared for each concentration of magnetite. To find out the difference between the concentration of magnetite and the increase of temperature, we

generated thermographs. The thermographs were plotted by using temperature increments recorded by temperature sensors, placed inside the phantom, during microwave radiation (300 s), and temperature sensor position (next to the antenna, at 0.5 cm, 1.0 cm and 1.5 cm). The cubic spline interpolation function of Matlab (Matworks inc. USA) was used to plot the thermograph; the values of the interpolation function were calculated every 0.1 cm. A thermochromatic sheet was placed close to the phantom to observe whether the radiation generated from the antenna was radial. Microwave radiation was applied five times for all the phantoms, and the temperatures with and without the MNPs were acquired every second during the experiments using True Temp software (Luxtron, USA). None of the phantoms was reused for the same experiment so that their electromagnetic and thermal properties were not affected.

3. RESULTS

3.1. Characterization of the Magnetic Nanoparticles

Figure 4 shows a TEM micrograph where one can observe the spherical shape of the magnetoliposomes (liposomes were not stained with uranyl acetate and, hence, only the magnetic particles inside the liposome are visualized)and the average diameter of 15 nm and 150 nm of the particles of ferrofluid and MLs, respectively.

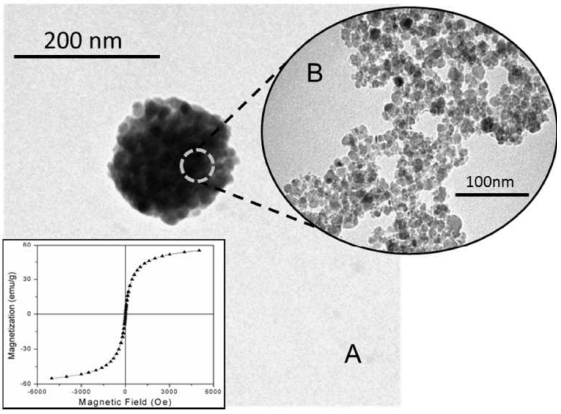

Figure 4. TEM image of: A) MLs and B) ferrofluid, shows the size and shape of particles. Inset: Magnetization curve for ferrofluid as a function of applied magnetic field.

The hydrodynamic diameter of the ferrofluid and MLs obtained by dynamic light scattering (DLS) was 52 ± 1 nm and 190 ± 1 nm, respectively. Both types of particles are nearly monodisperse: polydispersity index (PI) $= 0.181 \pm 0.003$ for ferrofluid, and 0.153 ± 0.015 for MLs. The average diameter obtained using this technique was much larger than that observed using TEM. This is because magneto static (magnetic dipole-dipole) interactions between particles can cause agglomeration even in the absence of any external magnetic field.

The Fe_3O_4 content of the ferrofluid and MLs was 22 mg/mL and 1.2 mg/mL, respectively. From these concentrations, the ferrofluid used in this study was diluted to see its thermal behavior at different concentrations.

The room temperature magnetization curve of the ferrofluid is shown in the inset of Figure 4. No hysteresis loop was observed, which indicated superparamagnetic behavior with a saturation magnetization of 52 emu/g. Furthermore, the coercive field was closed to zero.

3.2. Characterization of Agarose Tumor Phantoms

The tumor phantoms presented a permittivity of 55.88 and a conductivity of 2.88 S/m at 2.45 GHz. The reported dielectric constant of cancerous tissue was around 59 and its conductivity was about 2.5 S/m at 2.45 GHz [22]. As can be seen, the properties achieved in phantom showed similar values to those reported in the literature. The differences in the relative permittivity and conductivity observed were 3.12 units and 0.38 S/m, respectively.

3.3. Temperature Measurements in the Agarose Tumor Phantoms

Once a set of reference values was obtained, the effect of ferrofluid concentration on temperature was evaluated using the same experiment setup and conditions as for the reference assay.

3.4. Implant of Ferrofluid

Figure 5 shows the experimental results for the temperature rise as a function of time for various concentrations of ferrofluid.

The main parameter used to determine the heating of the tissue was the SAR, which is defined as the rate at which electromagnetic energy is absorbed by unit mass of a biological material and is proportional to the rate of the temperature increase ($\Delta T/\Delta t$) for adiabatic processes. From the initial slopes of the curves, SAR values

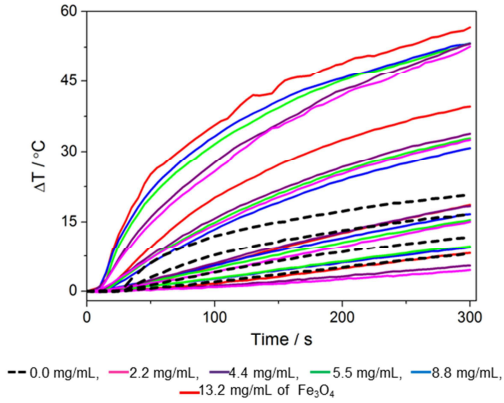

Figure 5. Temperature increments measured with the four fiber-optic sensors, placed inside the phantom, for each of the four concentrations of magnetite (in spheres of 1.5 cm) and in absence of MNPs. For each concentration, 4 time-dependent curves are displayed. Temperature was measured at the center of tumor phantom (highest temperatures for each concentration), next to the antenna, at 0.5 from the antenna, but still inside the tumor phantom, and at 1.5 cm and 2.0 from the antenna, both outside the tumor phantom (lowest temperatures for each concentration).

were calculated using

$$SAR = C_e \left(\frac{\Delta T}{\Delta t} \right)_{t=0}, \tag{5}$$

where C_e is the specific heat capacity of the sample. We used the specific capacity of a high water content tissue (3470 J/K kg) [23] because our phantom mimics this kind of tissue. The obtained SAR values for spheres of 2.5 mL were 1090 W/kg (2.2 mg/mL), 1166 W/kg (4.4 mg/mL), 1454 W/kg (5.5 mg/mL), 1544 W/kg (8.8 mg/mL), and 1697 W/kg (13.2 mg/mL). These values were plotted as a function of FF concentration, Figure 6; from this figure, it is evident the rise of SAR values associated with FF concentration.

Temperature increase distribution as a function of time, at the end of each test, is shown in Figure 7. Interpolation, in time and space, was used to make a graphical representation of the evolution in time of the four temperatures measured inside the phantom; the same method was carried out for Figures 8 and 9. As indicated above, it was verified, by means of a thermochromic paper, that the temperature gradient was radial. Then, by using the cubic spline interpolation function of

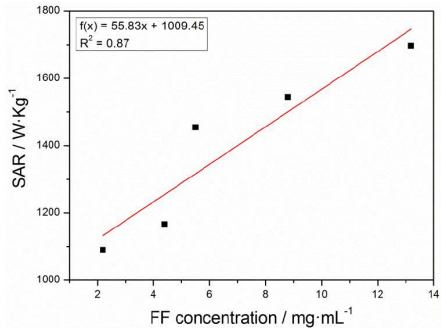

Figure 6. Plot of SAR as a function of ferrofluid concentration for 2.5 mL spheres.

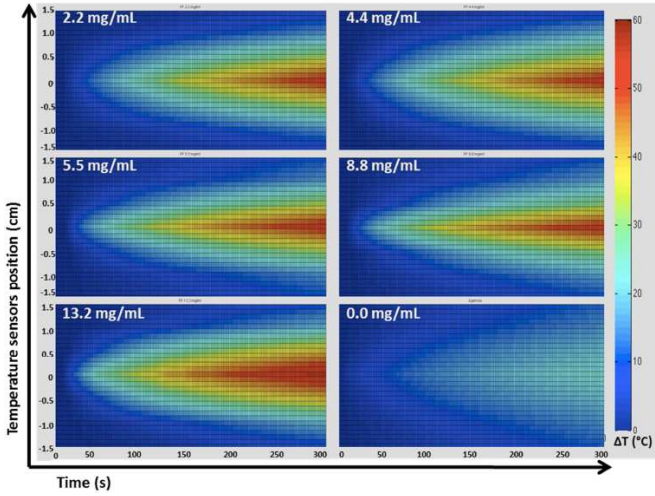

Figure 7. Temperature increase distribution as a function of time during 5 min at 10 W irradiation in phantoms with 2.5 mL spheres containing ferrofluid at different concentrations, from 0 to 13.2 mg/mL.

Matlab (Mathworks inc., USA) the figure was plotted. As can be seen, the increase in heating was concomitant with an increase in ferrofluid concentration. Maximum temperature increase was observed in the presence of ferrofluid at a concentration of 13.2 mg/mL of magnetite. Table 1 summarizes the temperature increments recorded at the end of each test for different positions of the fiber sensors with respect to the antenna for ferrofluid.

Table 1 shows that the same concentration of MNPs (8.8 mg/mL) but in a larger sphere (5 mL instead of 2.5 mL) resulted in a smaller increase in temperature. The corresponding thermograms show the difference in heat distribution clearly (Figure 8): with a sphere of 5 mL, the heat generated was distributed more homogenously throughout the phantom.

Table 1. Temperature increases in phantoms with different concentrations of ferrofluid and ML after 5 min of microwave irradiation. The volume used was 2.5 mL; *except for this case, 5 mL. ** Phantom without MNPs.

	Concentration /mg mL^{-1}	Sensor next to the antenna/°C	Sensor at 0.50 cm/°C	Sensor at 1.00 cm/°C	Sensor at 1.50 cm/°C
FF	13.2	56.64	39.57	18.62	8.13
	8.8	53.28	30.76	16.66	9.38
	8.8 *	32.29	21.46	19.26	7.27
	5.5	53.25	32.81	15.42	9.78
	4.4	53.19	33.78	18.36	5.40
	2.2	52.63	32.51	15.06	4.52
ML	1.2	53.44	32.64	14.64	5.35
	1.2*	23.13	18.37	17.90	11.00
	0**	20.78	16.65	11.75	7.99

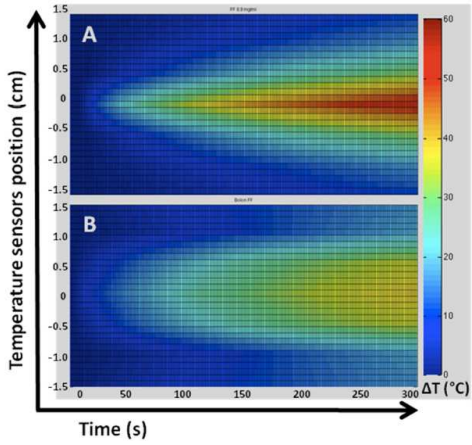

Figure 8. Temperature increase distribution as a function of time during 5 min at 10 W irradiation in phantoms with 8.8 mg/mL of magnetite containing ferrofluid: A) ferrofluid was inserted in a 2.5 mL sphere and B) ferrofluid was inserted in a 5 mL sphere.

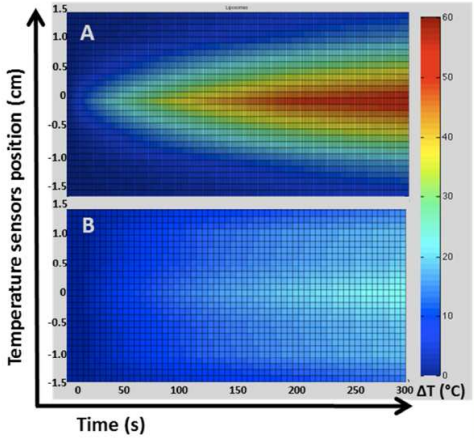

Figure 9. Temperature increment distribution as a function of time during 5 min at 10 W irradiation in phantom with MLs 1.2 mg/mL of magnetite A) MLs were inserted in a sphere of 2.5 mL and B) MLs were inserted in a sphere of 5 mL.

3.5. Implant of MLs

Values of SAR corresponding to magnetoliposomes were calculated by using Eq. [5] and were 1603 W/kg for a sphere of 2.5 mL, and 562 W/kg for one of 5 mL. The temperature distribution, in tumor phantom with MLs inside, is displayed in Figure 9. It is noteworthy that in spite of having encapsulated a lower concentration of magnetite (1.2 mg/mL), temperature increments were greater than those obtained with ferrofluid at a concentration of 8.8 mg/mL. A comparison of temperature distributions in spheres of different volumes showed similar behavior to the one observed for the ferrofluid. Table 1 shows the temperature increments recorded at the end of each test for different positions of the fiber sensors with respect to the antenna for MLs.

4. DISCUSSION

The heating effect caused by iron oxide nanoparticles subjected to an alternating magnetic field is caused by a combination of several different mechanisms: hysteresis loss, and Néel and Brownian relaxation. MNPs with a core diameter of less than 20 nm [24] have a single magnetic domain and have superparamagnetic properties. Under these particular conditions, the heating mechanism is dominated

by Brownian and Néel relaxation.

In hyperthermia treatment, controlling electromagnetic energy delivery to tumors is still a great challenge. This paper reports the heating effects in a tissue-mimicking phantom. In this study, ferrofluid and MLs were used as MNPs to focus EM energy in tumors [25]. The temperature recorded during treatment increased, although not in a linear way, with the increase of the concentration of MNPs into the sphere. The temperature increment was independent of concentration between 2.2–8.8 mg/mL; there were no differences between the final temperatures recorded with the different probes, but we observed little differences in the kinetics of heating: the final temperature for concentrations of 8.8 mg/mL and 5.5 mg/mLwas reached faster than for the concentrations of 4.4 mg/mL and 2.2 mg/mL. With a concentration of 13.2 mg/mL of magnetite, the highest temperature was achieved by the probe close to the antenna. The temperature difference between the probe that was next to the antenna and the one which was 2 cm from the antenna, outside the phantom that contained the nanoparticles, was approximately 50°C. The recorded temperature decreased with a decreasing concentration of nanoparticles and distance from the antenna. We observed that when the concentration was 0.0 mg/mL, there was no thermal ablation because the achieved temperature was lower than 50°C. We obtained a temperature increment of 20.78°C in the reference phantom, whose initial temperature was 25°C. When nanoparticles were used, we obtained greater increments in temperature than those observed in a reference phantom. Hence, nanoparticles do contribute to temperature increments. It is worth mentioning that the temperature may have increased more if radiation had been applied for longer times or at higher power rates. On the other hand, SAR determination showed the utility of the use of MNPs, since higher values of SAR were associated with an increase of FF concentration. The heating in the MLs was significantly higher for the same concentration of FF inside the liposome than for the FF alone. It has been described that the increase of thermal conductivity of nanoparticles in comparison to the macroscopic materials arises from the clustering of nanoparticles [26]. FF inside a liposome forms clusters and the effective volume of a cluster, i.e., the volume from which other clusters are excluded, can be much larger than the physical volume of the particles. Within such clusters, heat can move very rapidly and this produces a significantly increase of the thermal conductivity.

With this study we have demonstrated the feasibility of improving temperature increment and of focusing heat into the phantom using nanoparticles. Moreover, the physical properties of MNPs are such that they interact with the magnetic field generated by the antenna.

In consequence, the experimental results show that the use of MNPs is promising for *in vivo* treatments and justify further research to validate the techniques *in vitro* and *in vivo*. The phantom is only a model, and the propagation losses of body implanted antennas are different depending on the kind of tissue [27]. Hence, more research is still needed to establish how to guide the particles inside tumor cells; continued progress in nanotechnology research should result in this soon.

The antenna used in this study generated electric and magnetic fields; in conventional ablation treatment, only the electric field is taken into account because tissues interact weakly with magnetic fields. However, this situation changes dramatically when nanoparticles with superparamagnetic properties are present inside the tissue. In such a case, the electric field interacts with the electrical properties of the tissue (permittivity and conductivity) and the magnetic field interacts with the permeability of the MNPs. For this reason, it is possible to say that the presence of MNPs enhances the effect of the antenna by taking advantage of the magnetic fields. This allows more effective SAR distributions and hence requires lower power levels. Therefore, the use of MNPs in ablation therapy using microwaves is a good option as a method of focusing thermal energy.

5. CONCLUSION

By using ferrofluid and magnetoliposomes, it is possible to focus the heat in a tumor region until the appropriate therapeutic temperature is reached. The magnetic nanoparticles used in this study in combination with a microwave applicator enhance the temperature increment in order to produce therapeutic ablation in the tissue model. Comparing the behavior of both types of nanoparticles, magnetoliposomes achieved the desired temperature rise at a lower magnetite concentration than the ferrofluid.

ACKNOWLEDGMENT

Authors are grateful for the financial support given by the Spanish Ministerio de Ciencia e Innovación (MICINN) to the project MAT2009-13155-C04-03. Authors thank J. H. Zepeda Peralta for his invaluable technical assistance.

REFERENCES

1. Miltenyi, S., W. Muller, W. Weichel, and A. Radbruch, "High gradient magnetic cell separation with MACS," *Cytometry*, Vol. 11, 231–238, 1990.
2. Radbruch, A., B. Mechtold, A. Thiel, S. Miltenyi, and E. Pfluger, "High-gradient magnetic cell sorting," *Methods in Cellular Biology*, Vol. 42, 387–403, 1994.
3. Safarik, I. and M. Safarikova, "Use of magnetic techniques for the isolation of cells," *Journal of Chromatography B: Biomedical Sciences and Applications*, Vol. 722, 33–53, 1999.
4. Swan, H., *Thermoregulation and Bioenergetics*, Elsevier, Amsterdam, 1974.
5. Suit, H. and M. Shwayder, "Hyperthermia: Potential as an antitumour agent," *Cancer*, Vol. 34, 122–129, 1974.
6. Hahn, G., *Hyperthermia and Cancer*, Plenum Press, New York, 1982.
7. Kettering, M., J. Winter, M. Zeisberger, S. Bremer-Streck, H. Oehring, C. Bergemann, C. Alexiou, R. Hergt, K. J. Halbhuber, W. A. Kaiser, and I. Hilger, "Magnetic nanoparticles as bimodal tools in magnetically induced labeling and magnetic heating of tumour cells: An *in vitro* study," *Nanotechnology*, Vol. 18, 175101, 2007.
8. Simon, C. J., D. E. Dupuy, and W. W. Mayo-Smith, "Microwave ablation: Principles and applications," *Radio Graphics*, Vol. 25, S69–S83, 2005.
9. Safarik, I. and M. Safarikova, "Magnetic nanoparticles in biosciences," *Monatschefte für Chemie*, Vol. 133, 737–759, 2002.
10. Saiyed, Z. M., S. D. Telang, and C. N. Ramchand, "Application of magnetic techniques in the field of drug discovery and biomedicine," *BioMagnetic Research and Technology*, Vol. 1, 2, 2003.
11. Diederich, C. J., "Thermal ablation and high-temperature thermal therapy: Overview of technology and clinical implementation," *International Journal of Hyperthermia*, Vol. 21, 745–753, 2005.
12. Oura, S., T. Tamaki, I. Hirai, T. Yoshimasu, F. Ohta, R. Nakamura, and Y. Okamura, "Radiofrequency ablation therapy in patients with breast cancers two centimeters or less in size," *Breast Cancer*, Vol. 14, 48–54, 2007.
13. Rosensweig, R. E., "Heating magnetic fluid with alternating magnetic field," *Journal of Magnetism and Magnetic Materials*,

Vol. 252, 370–374, 2002.

14. Rovers, S. A., R. Hoogenbomm, M. F. Kemmere, and J. T. F. Keurentjes, "Relaxation processes of superparamagnetic iron oxide nanoparticles in liquid and incorporated in poly (methyl methacrylate)," *Journal of Physical Chemistry C*, Vol. 112, 15643–15646, 2008.
15. Pankurst, Q. A., J. Connolly, S. K. Jones, and J. Dobson, "Applications of magnetic nanoparticles in biomedicine," *Journal of Physics D: Applied Physics*, Vol. 36, R167–R181, 2003.
16. Huang, H., F. H. Xue, B. Lu, F. Wang, X. L. Dong, and W. J. Park, "Enhanced polarization in tadpole-shaped (Ni, Al)/Aln nanoparticles and microwave absorption at high frequencies," *Progress In Electromagnetics Research B*, Vol. 34, 31–46, 2011.
17. Hergt, R. and W. Andrä, "Magnetic hyperthermia and thermoablation," *Magnetism in Medicine*, 2nd Edition, W. Andrä and H. Nowak, editor, Wiley-VCH, Berlin, 2007.
18. Lai, J. C. Y., C. B. Soh, E. Gunawan, and K. S. Low, "Homogeneous and heterogeneous breast phantoms for ultra-wideband microwave imaging applications," *Progress In Electromagnetics Research*, Vol. 100, 397–415, 2010.
19. Sabaté, R, R. Barnadas-Rodríguez, J. Callejas-Fernández, R. Hidalgo-Álvarez, and J. Estelrich, "Preparation and characterization of extruded magnetoliposomes," *International Journal of Pharmaceutics*, Vol. 347, 156–162, 2008.
20. Cepeda, M. F. J., A. Vera. and L. Leija, "Coaxial antenna for microwave coagulation therapy in ex vivo swine breast tissue," *7th International Conference on Electrical Engineering, Computing Science and Automatic Control (CCE 2010)*, Tuxtla Gutiérrez, Chiapas, México, Sept. 8–10, 2010.
21. Trujillo-Romero, C. J., S. García-Jimeno, A. Vera, L. Leija, and J. Estelrich, "Using nanoparticles for enhancing the focusing heating effect of an external waveguide applicator for oncology hyperthermia: Evaluation in muscle and tumor phantoms," *Progress In Electromagnetics Research*, Vol. 121, 343–363, 2011.
22. Lazebnik, F. M., D. Popovic, L. McCartney, C. B. Watkins, M. J. Lindstrom, J. Harter, et al., "A large-scale study of the ultrawideband microwave dielectric properties of normal, benign and malignant breast tissues obtained from cancer surgeries," *Physics in Medicine and Biology*, Vol. 52, 6093–6115, 2007.
23. Guy, A. W., "Analysis of electromagnetic fields induced in biological tissues by thermographic studies on equivalent

phantom models," *IEEE Transactions in Microwave Theory and Techniques*, Vol. 19, 205–214, 1971.

24. Leslie-Peleckie, D. L. and R. D. Rieke, "Magnetic properties of nanostructured materials," *Chemistry of Materials*, Vol. 8, 1770–1783, 1996.
25. Iero, D., T. Isernia, A. F. Morabito, I. Catapano, and L. Crocco, "Optimal constrained field focusing for hyperthermia cancer therapy: A feasibility assessment on realistic phantoms," *Progress In Electromagnetics Research*, Vol. 102, 125–141, 2010.
26. Keblinski, P., S. R. Phillpot, S. U. S. Choi, and J. A. Eastman, "Mechanisms of heat flow in suspensions of nano-sized particles (nanofluids)," *International Journal of Heat and Mass Transfer*, Vol. 45, 855–863, 2002.
27. Gemio, J., J. Parrón, and J. Soler, "Human body effects on implantable antennas for ISM bands applications: Models comparison and propagation losses study," *Progress In Electromagnetics Research*, Vol. 110, 437–452, 2010.